Electronic Supplementary Material (ESI) for Journal of Materials Chemistry C.
This journal is © The Royal Society of Chemistry 2017

Enhanced physical properties of pulsed laser deposited NiO films via annealing and lithium doping for improving perovskite solar cell efficiency

Zhiwen Qiu[a, b], Haibo Gong[a], Guanhaojie Zheng[b], Shuai Yuan[a,], Hailiang Zhang[a], Xiaomeng Zhu[a], Huanping Zhou[b,†], Bingqiang Cao[a,†]

[a] *Materials Research Center for Energy and Photoelectrochemical Conversion, School of Material Science and Engineering, University of Jinan, Jinan 250022, Shandong, China.*

[b] *Department of Materials Science and Engineering, College of Engineering, Peking University, Beijing 100871, China.*

† *To whom all correspondence should be addressed.*

Mse_caobq@ujn.edu.cn; happy_zhou@pku.edu.cn

1. Experimental Section

1.1 Growth of NiO and Li-doped NiO thin films by pulsed laser deposition

NiO targets doped with Li_2O of different atomic concentration (0–20 mol%) made from 5 N powders were first pressed under 7 MPa and then sintered at 1000 ^{o}C for 10 hrs. KrF excimer laser (Coherent, CompexPro 205) pulse with a 5 Hz repetition frequency was applied for PLD growth. The laser energy density focused on the target was about 2 Jcm^{-2}. Indium-doped tin oxide (ITO)-coated glass (15 Ω sq^{-1}, Pilkington) was used as substrate for the film growth. NiO layer was deposited with an O_2 pressure of 0.013 Pa–13 Pa at ambient temperature. High purity oxygen was used as the carrier gas at a constant flow rate of 8 SCCM (stand cubic centimeter per minutes). The distance between target and substrate was 100 mm. Then the NiO films were post-annealed under different temperature (100 ^{o}C–450 ^{o}C) for 20 min in a rapid annealing furnace.

1.2 Fabrication of $CH_3NH_3PbI_{3-x}Cl_x$ perovskite solar cells

ITO glass was patterned by etching with Zn powder and 2 M HCl diluted in deionized water. The sheets were then washed with soap (2% Hellmanex in water), deionized water, acetone, and methanol. Finally, the substrates were further treated under oxygen plasma for 15 min to remove the residual traces of organic residues. PbI_2 and $PbCl_2$ (1 M, molar ratio of 2:1, Sigma-Aldrich) were dissolved in anhydrous N,N-dimethylformamide (DMF, Sigma-Aldrich). The solution was stirred at 70 ^{o}C overnight to encourage complete dissolution, cooled to room temperature, and then

filtered through a 0.45 μm PTFE filter before use. CH_3NH_3I (70 mg/ml, Sigma-Aldrich) was dissolved in anhydrous 2-propanol (IPA, Sigma-Aldrich). Then PCBM (Sigma-Aldrich) was dissolved in a chlorobenzene solution with 15 mg/ml.

Perovskite $CH_3NH_3PbI_{3-x}Cl_x$ films were prepared with the two-step sequential deposition method.[1] The solar cell devices were fabricated with the structure of ITO/NiO/$CH_3NH_3PbI_{3-x}Cl_x$/PCBM/Ag. A NiO layers prepared by PLD at room-temperature were then annealed in air under different temperature ranging from 100 ^oC to 450 ^oC. We used a mixture of $PbCl_2$ and PbI_2 solution as the precursor, and spin-coated at 4000 rpm on the compact NiO film. Then a drop of 70 mg/ml CH_3NH_3I solution was added onto the middle of $PbI_{2-x}Cl_x$ film and the substrate was further spinning at 4000 rpm for 30 s. The film color changed from chartreuse to dark brown, indicating the formation of perovskite $CH_3NH_3PbI_{3-x}Cl_x$ film. It was also annealed in N_2 at 100 ^oC for 30 min. Then, PCBM was coated onto the perovskite layer at 2500 rpm for 30 s. Finally, the devices were transferred into a vacuum chamber for Ag electrode deposition through a shadow mask. The active area of the Ag electrodes in the fabricated device was 7.5 mm^2.

1.3 Materials and device characterizations

The morphology, composition and crystal structure of the films and devices were characterized by scanning electron microscope (SEM, QUANTA FEG250), X-ray photoelectron spectroscopy (XPS, ESCALAB 250, THERMOFISHER SCIENTIFIC) with a HeI (21.2 eV for UPS) discharge lamp and X-ray diffraction (XRD, D8-ADVANCE; BRUKER). For photoluminescence (PL) measurements, 450 nm diode

laser was used as excitation source. The light beam was focused on the sample through an optical chopper (SR 540). The PL signal dispersed by a monochrometer was detected by a photomultiplier (PMTH–S1–CR131) through a lock-in amplifier (SR 830). The absorption and transmission spectra were examined by a UV–vis–NIR spectrophotometer (UV–3600, Shimadzu). Raman scattering spectrum was measured under 532 nm diode laser excitation at room temperature (LabRAM HR Evolution). Current-voltage (*J–V*) characteristics of solar cells were measured using a Keithley 2400 source measure unit under a simulated AM1.5G spectrum (3A, San–Ei). The external quantum efficiency (EQE) was measured with a QEX10 system (PV Measurement). Impedance spectroscopic measurements (ZAHNER ENNIUM) were performed with a 10 mV rms amplitude over the frequency range of 1 Hz to 1 MHz under 100 mW/cm^2. ZSimDemo Analyst software was used to model the Nyquist plots obtained from the impedance measurements.

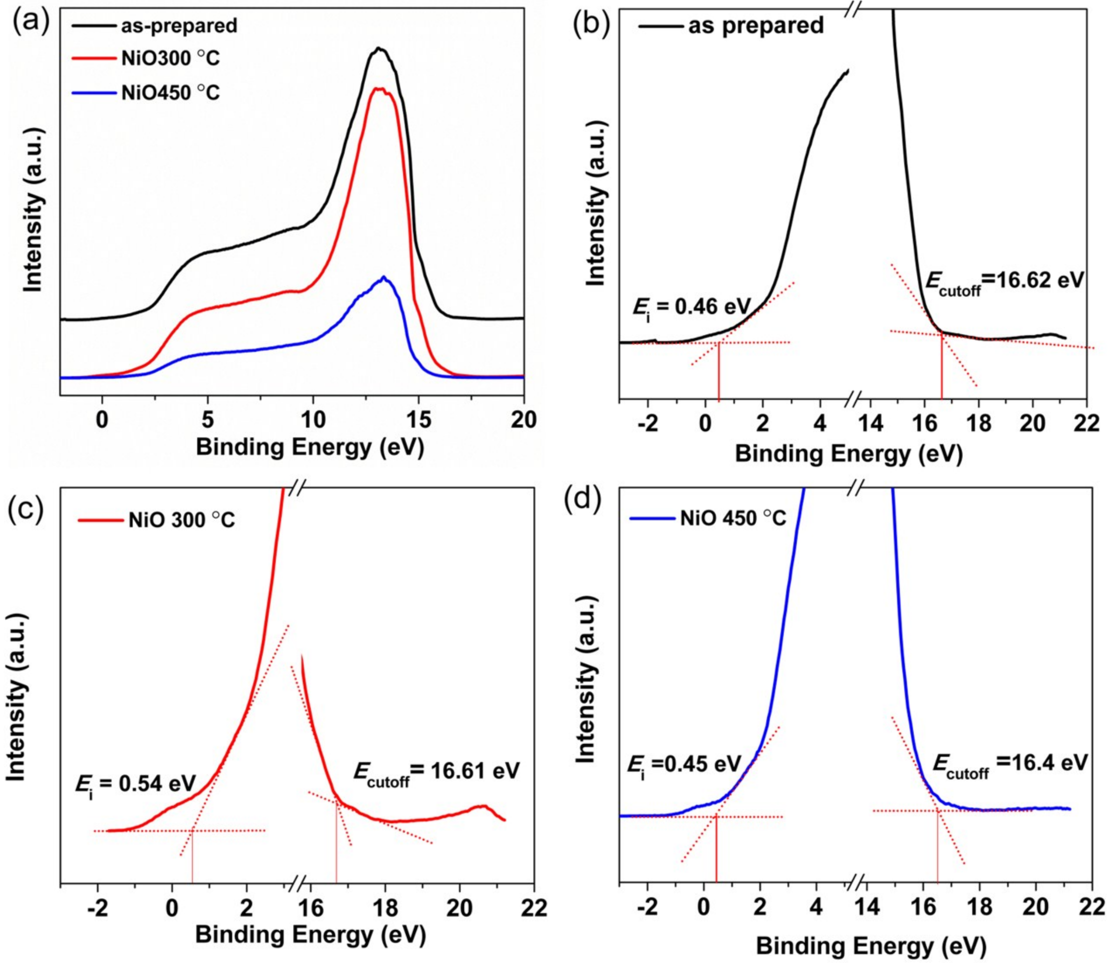

Fig. S1 (a-d) UPS spectra of the NiO based charge extraction layers without annealing and annealed under 300 °C and 450 °C.

The energy difference (E_i) between the valance band maximum (E_{VB}) and E_F is derived from the low binding energy tails (in the range below 4 eV). The work function, or Fermi level (E_F) of the charge carrier extraction layers are obtained by subtracting the binding energies of the secondary electron cutoffs (in the range of 16–18 eV) from the excitation energy (21.2 eV) of HeI UPS spectra. The position of the valence band could be confirmed using the equation $E_{VB} = 21.2–(E_{cutoff} - E_i)$.[2] When the annealing temperature increases from R.T. to 450 °C, the E_{VB} varies from -5.04 eV, -5.13 eV to -5.25 eV. Conduction band (E_{CB}) edge values is obtained by adding the optical band gaps (E_g =3.75 eV) to E_{VB}. The difference between the valence band

and Fermi level of NiO layers is ~0.5 eV, based on the valence band spectra provided in Fig. S1. This confirms the p-type nature of the NiO oxide.[3]

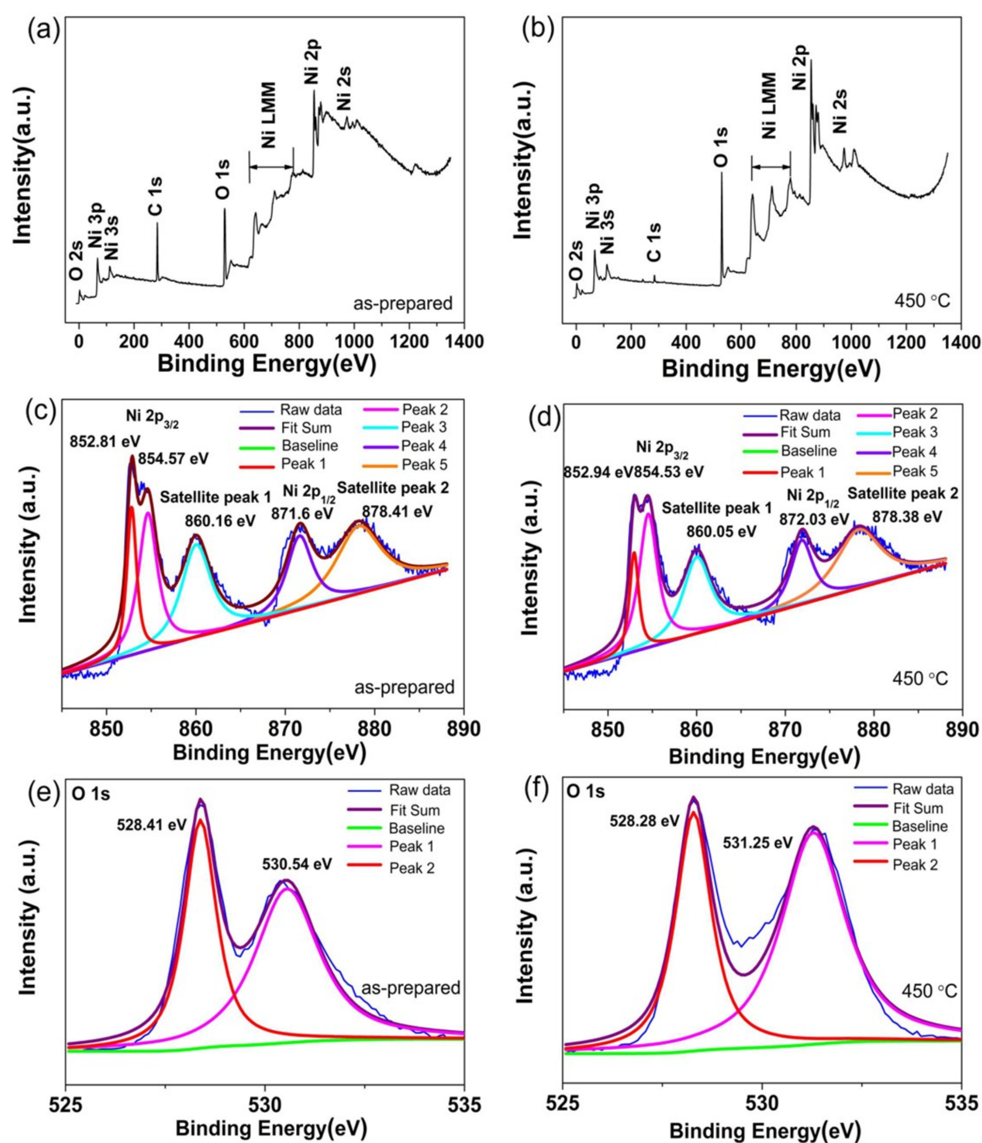

Fig. S2 X-ray photoelectron survey spectra of as-prepared NiO film (a) and annealed under 450 °C NiO film (b); high-resolution X-ray photoelectron spectra of Ni 2p and O 1s core level of as-prepared NiO film (c, e) and annealed under 450 °C NiO film (d, f).

Table S1 Ni2p analysis of as-prepared and annealed under 450 ^{o}C NiO films.

NiO	Peak	Position *BE*(eV)	FWHM	Raw area (cps eV)	At. %
as-prepared	Peak (1)	852.81	1.31	27740.41	12.4
	Peak (2)	854.62	2.55	50195.69	22.44
	Peak (3)	860.02	3.94	52450.1	23.45
	Peak (4)	871.59	3.4	35840.28	16.02
	Peak (5)	878.19	5.95	57455.66	25.69
450 ^{o}C	Peak (1)	852.94	1.25	17940.64	9.69
	Peak (2)	854.54	2.5	48312.52	26.11
	Peak (3)	860.01	3.72	41359.12	22.35
	Peak (4)	871.86	2.96	27417.17	14.82
	Peak (5)	878.26	5.91	50015.8	27.03

Table S2 O1s analysis of as-prepared and annea1ed under 450 ^{o}C NiO films.

	Peak	Position *BE*(eV)	FWHM	Raw area (cps eV)	At. %
as-prepared	Peak (1)	528.39	1.21	28566.1	48.39
	Peak (2)	530.38	1.92	30424.09	51.61
450 ^{o}C	Peak (1)	528.28	1.31	36808.13	39.3
	Peak (2)	531.25	2.33	56731.77	60.7

Table S3 Summary of Ni/O ratio of NiO films of as-prepared and annealed under 450 ^{o}C.

NiO	NiAt. (%)	O At. (%)	Ni/O ratio
as-prepared	32.34	67.66	0.48
450 ^{o}C	26.58	73.42	0.36

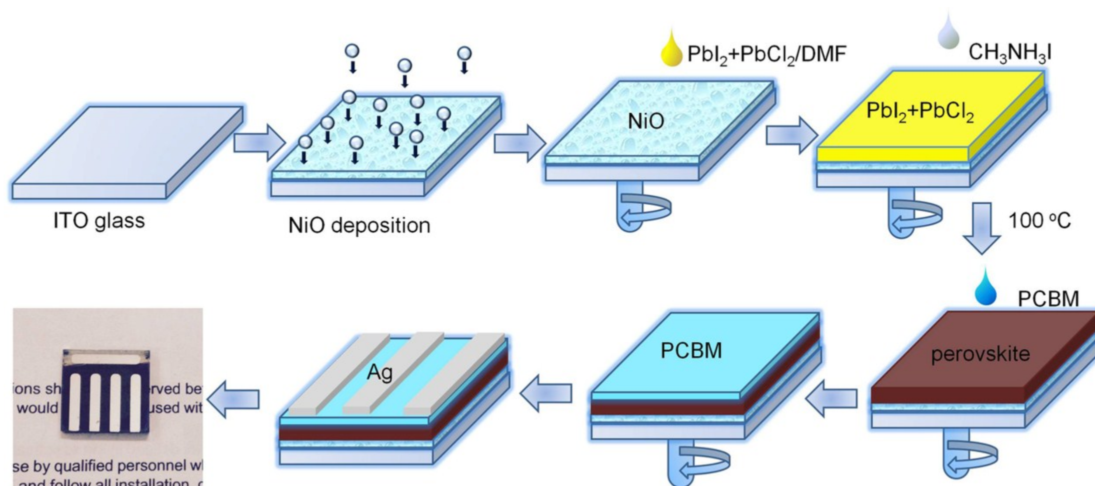

Fig. S3 Schematic illustration of perovskite solar cells fabricated by the two-step sequential deposition method.

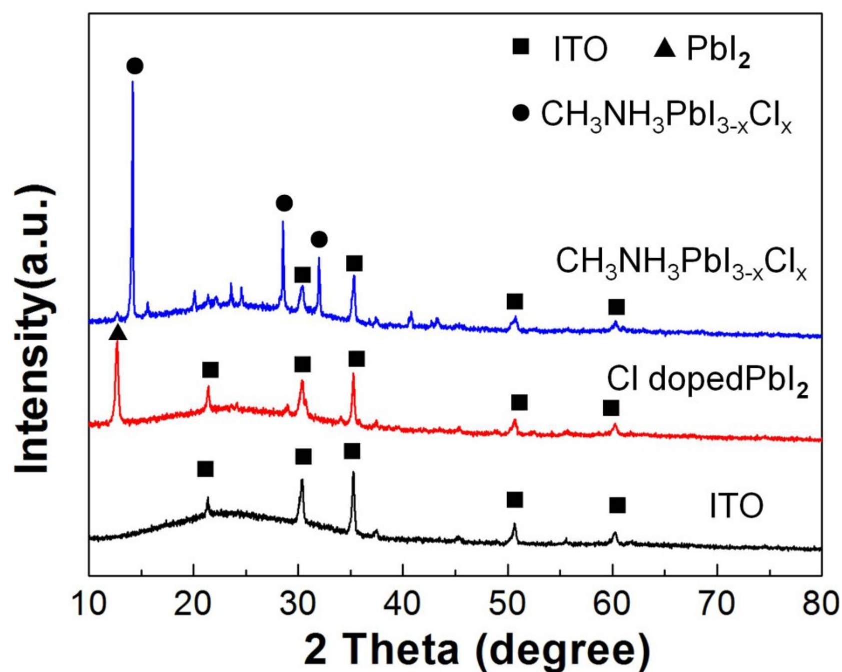

Fig. S4 XRD patterns of ITO, Cl doped PbI_2 and $CH_3NH_3PbI_{3-x}Cl_x$ deposited on a compact NiO/ITO substrate.

Fig. S4 shows the XRD spectra of the ITO glass substrate, Cl doped PbI_2, and $CH_3NH_3PbI_{3-x}Cl_x$ films on the NiO-coated ITO substrates. For the Cl doped PbI_2 film, the peak at 12.7° belongs to (001)-orientation of PbI_2 film (denoted by triangle). After the perovskite film growth, characteristic diffraction peaks (denoted by circle) at about 14.1°(110), 28.4°(220), 31.8° (310) from $CH_3NH_3PbI_{3-x}Cl_x$ crystal planes are observed.[4] The other XRD peaks are attributed to the ITO substrate and no secondary

phase (e.g., PbI_2) is found.

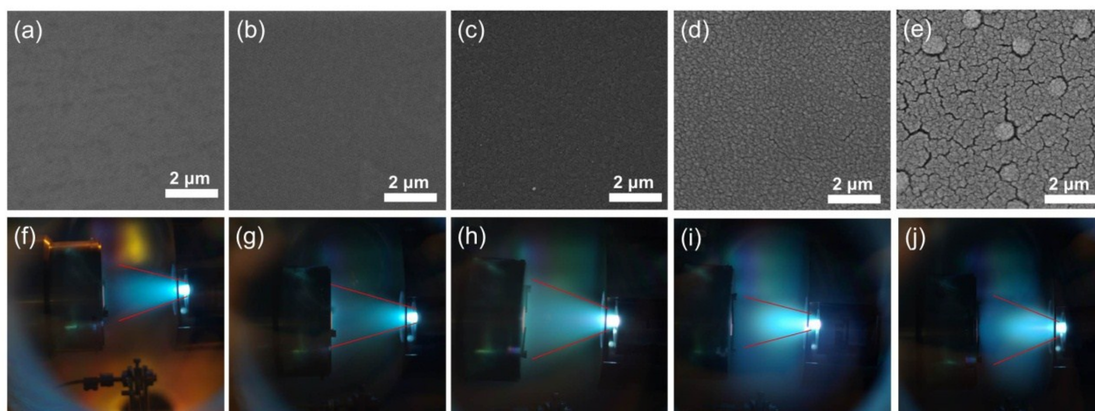

Fig. S5 SEM images showing the general morphology of NiO films under different oxygen pressure (a-e). (a) 0.013 Pa; (b) 0.65 Pa; (c) 1.3 Pa; (d) 6.5 Pa; (e) 13 Pa; (f-j) evolution of the corresponding plasma plume under different oxygen pressure change from 0.013 Pa–13 Pa.

Table S4 Resistivity of NiO thin films as a function of oxygen pressure.

Oxygen pressure (Pa)	0.013 Pa	0.65 Pa	1.3 Pa	6.5 Pa	13 Pa
Resistivity	∞	90 MΩ	12 MΩ	∞	∞

Oxygen pressure is a key parameter for the growth of NiO thin films by PLD, which has a significant effect on the morphology and physical property of NiO films, and will further influence the performance of perovskite solar cell devices. With the increase of oxygen partial pressure (0.013 Pa–13 Pa) in Fig. S5(a-e), the roughness of the surface increases. But, for high oxygen partial pressure shown in Fig. S5(d–e), a lot of large particles accumulate on the films surface and the films become extremely rough. The film surface difference is mainly due to the collision between NiO ion plasma plume and oxygen molecules at different oxygen pressure. It affects the quality of thin film crystallization and a large number of particles appear on the film surface.[5] The corresponding changes of plasma plume under different oxygen pressure are also illustrated in Fig. S5. Resistivity at 1.3 Pa is the minimum.

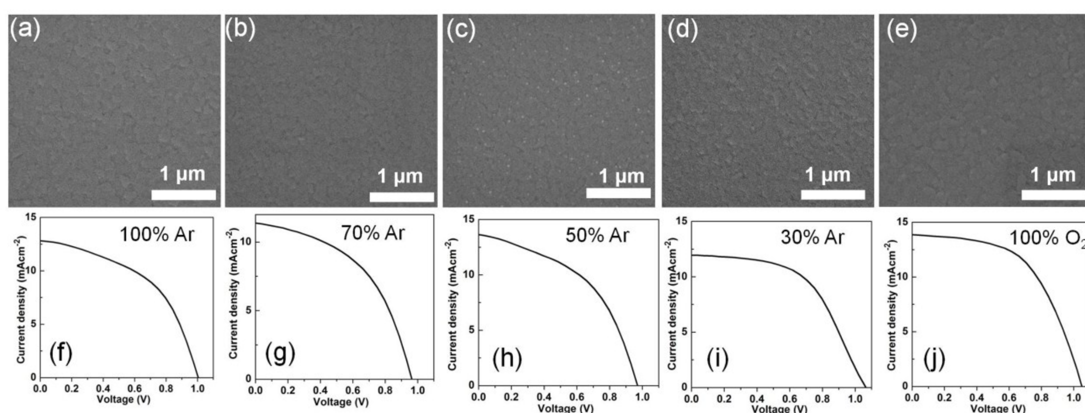

Fig. S6 SEM images showing the general morphology of NiO films under different atmosphere (a-e). (a)100% Ar; (b) 70% Ar (30% O_2); (c) 50% Ar (50% O_2); (d) 30% Ar (70% O_2); (e) 100% O_2; (f-j) The corresponding photocurrent density–voltage (*J–V*) curves of perovskite solar cells based on PLD-NiO films under different atmosphere.

Table S5 Photovoltaic parameters of the PLD-NiO-based perovskite solar cells as a function of atmosphere.

atmosphere	V_{oc} (V)	J_{sc} (mA/cm^2)	FF (%)	PCE (%)
100% Ar	1.0	12.85	48.9	6.35
70% Ar (30% O_2)	0.96	11.39	48.6	5.38
50% Ar (50% O_2)	0.97	13.64	47.2	6.3
30% Ar (70% O_2)	1.06	11.94	53.7	6.9
100% O_2	1.05	13.87	54.76	8.0

In order to study the effects of NiO thin film prepared under different working gas environments on the photovoltaic performance, the *J–V* characteristics of the PLD-NiO/$CH_3NH_3PbI_{3-x}Cl_x$/PCBM/Ag heterojunction cells are demonstrated. The stoichiometry and therefore the properties of NiO thin film are controlled by adjusting the ratio of working gases (Ar and O_2) in the vacuum chamber during pulsed laser deposition method process. In fact, in this study, the change of the Ar/O ratio would

not affect the photovoltaic performance obviously, which can be shown in Table S6. The highest efficiency up to 8.0% (under AM1.5G irradiation) is achieved for the cell based on NiO hole transport layer prepared under pure O_2 working gas. So in further experiments, we adapt only O_2 as working gases.

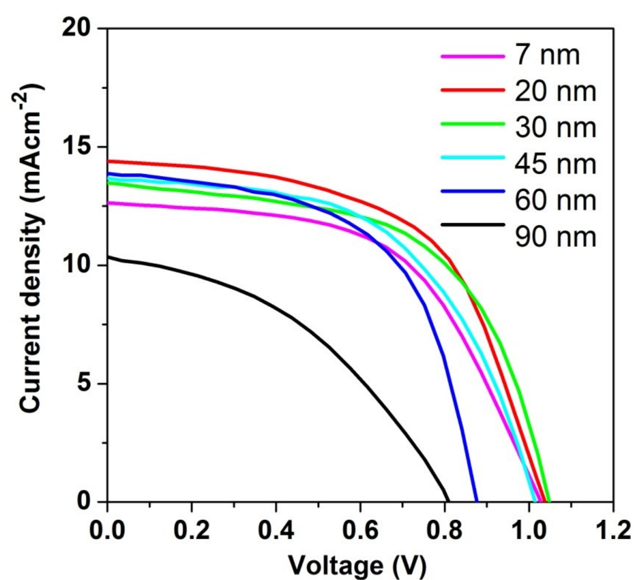

Fig. S7 The photocurrent density–voltage (*J*–*V*) curves of perovskite solar cells based on PLD-NiO films of different thickness.

Table S6 Photovoltaic parameters of the PLD-NiO-based perovskite solar cells as a function of different thickness.

Buffer layer	Thinckness (nm)	V_{oc} (V)	J_{sc} (mA/cm^2)	FF (%)	PCE (%)
NiO	7 nm	1.03	12.64	55.26	7.26
	20 nm	1.04	14.39	56.82	8.49
	30 nm	1.04	14.17	56.07	8.37
	45 nm	1.02	13.67	54.33	7.62
	60 nm	0.88	13.87	57.79	7.10
	90 nm	0.81	10.35	41.45	3.51

To probe the effect of NiO film thickness on device performance, devices are fabricated on 200 ^oC annealed NiO thin films of different thickness (Fig. S7 and Table S6). All other PLD parameters remain unchanged with a constant repetition frequency of 5 Hz and controlling the oxygen partial pressure of 1.33 Pa. The current-voltage (J–V) characteristics of the PLD-NiO/$CH_3NH_3PbI_{3-x}Cl_x$/PCBM heterojunction cells are shown in Fig. S7. As mentioned above, the best device demonstrates a short-circuit current (J_{sc}) of 14.39 mA cm^{-2}, open circuit voltage (V_{oc}) of 1.04 V, fill factor (FF) of 56.82, and a power conversion efficiency (PCE) of 8.49%. This implies that the PLD-prepared thin NiO film of 20 nm works well as HTL because of the high optical transparency and the sufficient energy level for hole extraction. It is found that the devices with NiO film of 7 nm, which might be caused by the unsatisfactory coverage of the thin NiO film on the ITO substrate. It is further found that the intrinsic photon absorption by NiO is likely to be the dominant factor affecting the device performance when the NiO layer of 90 nm is used. Therefore, we choose the NiO film of 20 nm for device fabrication in the following discussion.

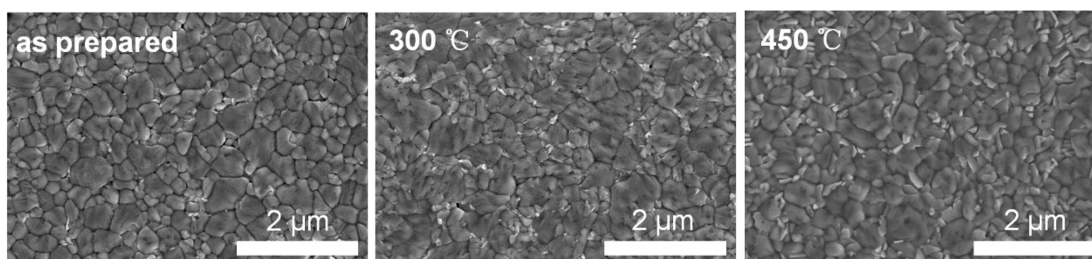

Fig. S8 Scanning electron microscopy (SEM) images of perovskite films on NiO films annealed under different temperature by two-step spin-coating process.

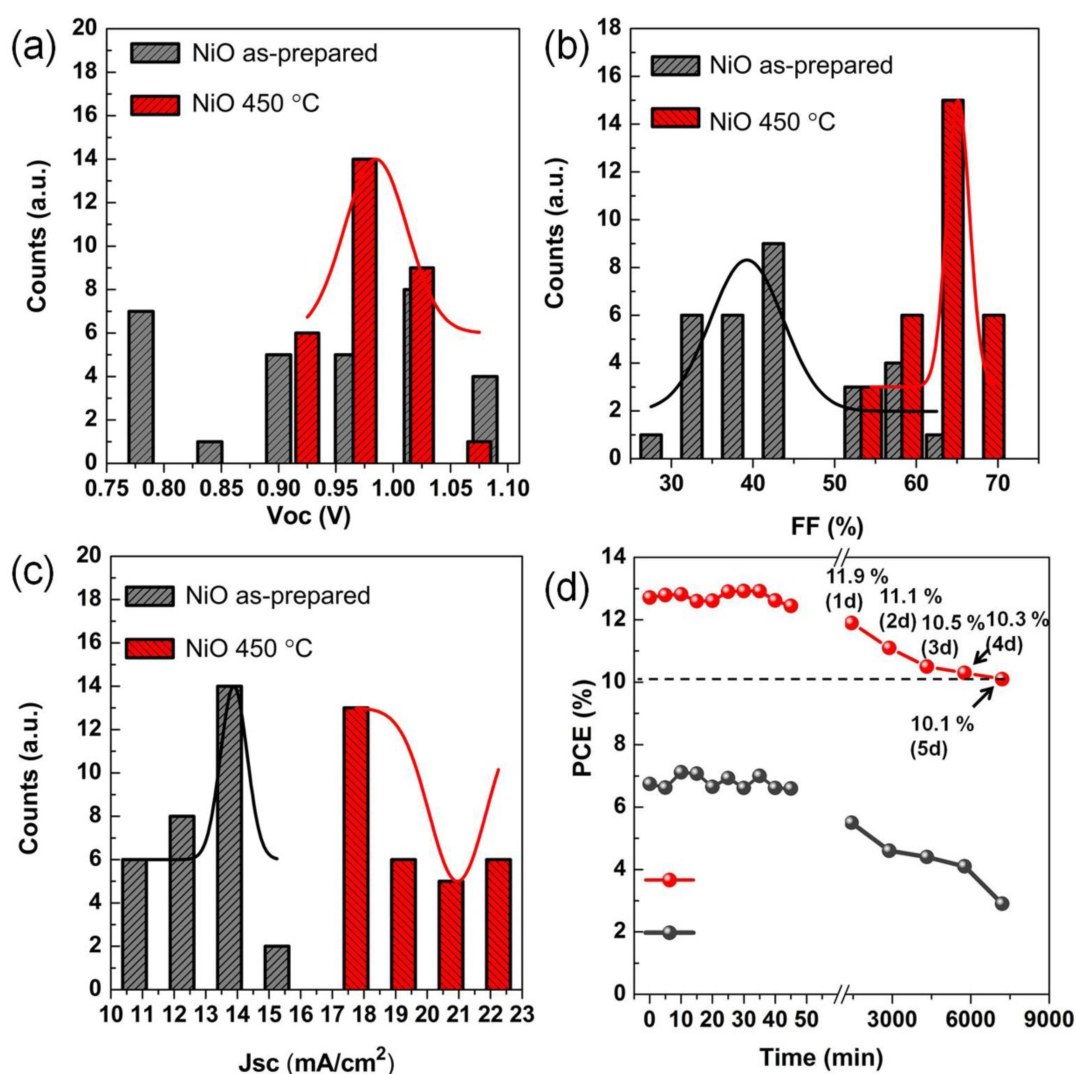

Fig. S9 (a-c) Current density (J_{sc}), fill factor (FF), open-circuit voltage (V_{oc}) depending NiO films without annealing and annealed under 450 ^{o}C; (d) Power conversion efficiency (PCE) of PLD-NiO based device stored for different numbers of days. The device without encapsulation is stored in dry box (RH about 1%) for long term stability measurement.

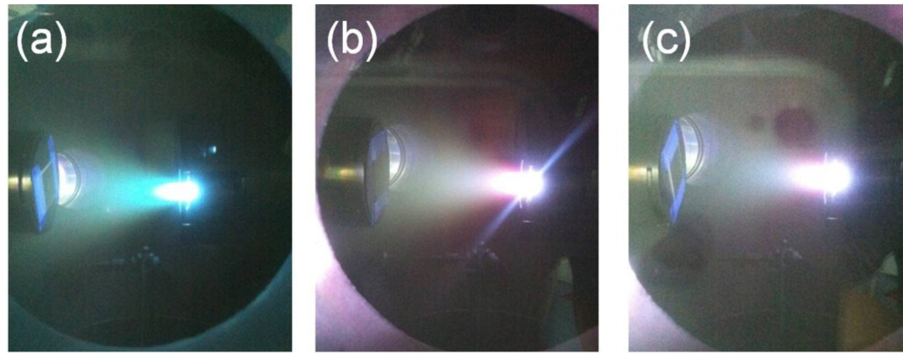

Fig. S10 Plasma plume photos of pulse laser ablated different NiO:Li*x* targets.

Table S7 Square resistance of the PLD-NiO:Li*x* films, where x = 0, 0.1, and 0.2 under different annealing temperature.

Buffer layer	Annealing Temperature (^{o}C)	Atmosphere	Pressure (Pa)	Square resistance (Ω/□)
NiO	as-prepared	O_2	1.33	4.17E+07
	200	O_2	1.33	3.01E+07
	450	O_2	1.33	6.40E+06
$NiO:Li_{0.1}$	as-prepared	O_2	1.33	9.43E+06
	200	O_2	1.33	9.50E+05
	450	O_2	1.33	7.20E+05
$NiO:Li_{0.2}$	as-prepared	O_2	1.33	4.01E+05
	200	O_2	1.33	2.40E+05
	450	O_2	1.33	1.63E+05

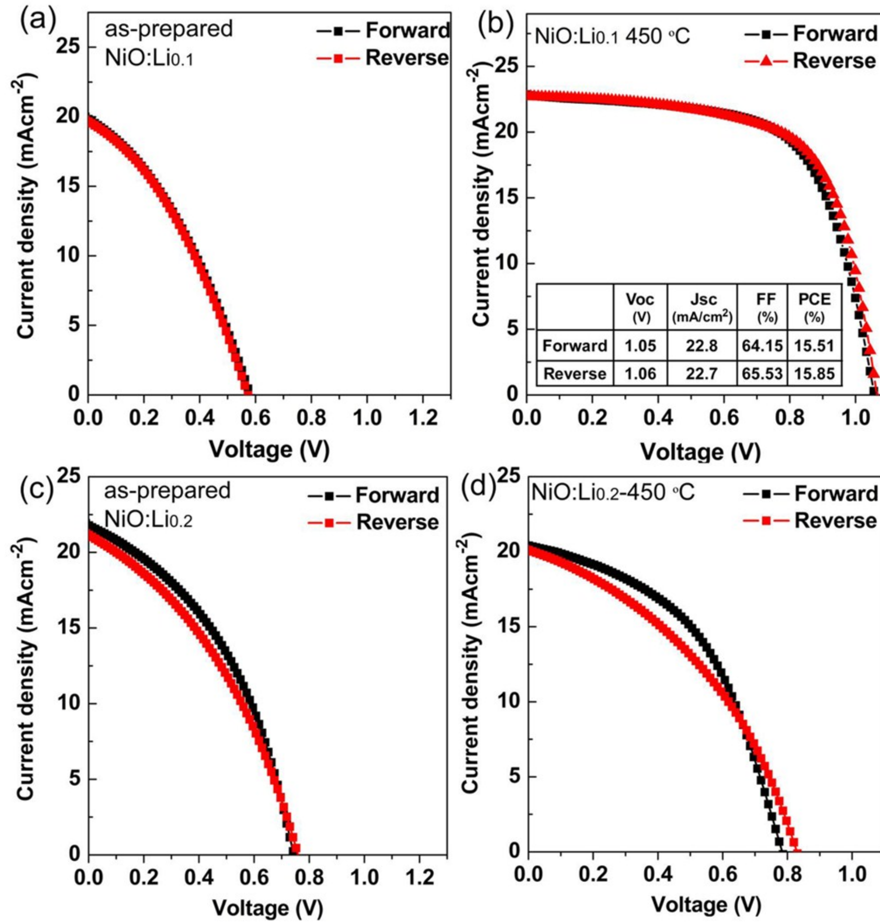

Fig. S11 (a)-(d) The photocurrent density–voltage (J–V) curves of perovskite solar cells based on PLD-NiO:Lix films, where x=0.1 and 0.2 without annealing and annealed under 450 ^{o}C.

Table S8 Photovoltaic parameters of perovskite solar cells based on PLD-NiO:Lix films, where x=0.1 and 0.2 without annealing and annealed under 450 ^{o}C.

Buffer layer	Annealling temperature (^{o}C)	V_{oc} (V)	J_{sc} (mA/cm^2)	FF (%)	PCE (%)
$NiO:Li_{0.1}$	as-prepared	0.58	19.84	35.05	4.03
	450	1.06	22.87	64.15	15.51
$NiO:Li_{0.2}$	as-prepared	0.74	21.79	41.31	6.69
	450	0.78	20.41	47.25	7.56

Herein, we study systematically the effect of different annealing temperature on the

electrical properties of NiO:Li_x thin films (where x = 0.1, 0.2) grown by PLD, which show great influence on the photovoltaic efficiency of the $CH_3NH_3PbI_{3-x}Cl_x$-based perovskite solar cells when NiO:Lix films are used as HTLs. In general, compared to the pristine NiO film, the conductivity of the Li doping film is increased by one to two orders of magnitude in Table S7. Also, electrical performance of all samples improve after annealing process. Detailed data is listed in the Table S7. When the annealing temperature increases from R.T. to 450 ^{o}C, for pristine NiO film, the square resistance decreases from 4.17×10^7 **Ω/□** to 6.40×10^6 **Ω/□**. Also the above XPS analysis in Fig.S2 can support well the electrical properties of NiO film. The J–V characteristics of the PLD-NiO:Lix/$CH_3NH_3PbI_{3-x}Cl_x$/PCBM heterojunction cells are demonstrated, which are shown in Fig. S11(a-d). Their device parameters are summarized in Table S8. For the device with as-prepared NiO:$Li_{0.1}$ film, both the forward scan and reverse scan output very low power conversion efficiency due to the ultra-small fill factor (FF, <0.36) and open circuit voltage (V_{OC}, <0.6 V). As expected, the device with NiO:$Li_{0.1}$film annealed at 450 ^{o}C shows significant enhancement in the J_{sc}, FF, V_{oc} and PCE value compared to that based on as-prepared NiO film. When increase the annealing temperature NiO:$Li_{0.1}$ from R.T to 450 °C, the PCE increases from 4.03% to 15.51% with an increase in the value of J_{SC} from 19.84 to 22.87 mA cm^{-2} and in the value of FF from 35.05% to 64.15% and in the value of V_{OC} from 0.58 V to 1.06 V. This phenomenon indicates that Li atoms without annealing process do not have enough energy to substitute Ni atoms and prefer to stay in the interstitial states.[7–8] After 450 ^{o}C annealing, higher temperature promotes the interstitial Li to

formation of Li_{Ni} (Li atom substitute Ni atom) and release the stress of crystal. Also, the surface and crystallization of $NiO:Li_{0.1}$ film become better. Performance is significantly improved after doping NiO film which increases their electrical conductivity and then reduces the carrier transport loss in the HTL. With the increase of Li concentration, too much Li doping introducing more defects deteriorates the crystal quality of $NiO:Li_{0.2}$ film.[9] No device performance improvements are observed although after high temperature annealing. The results are consistent with Table S7.

References

[1] J. Burschka, N. Pellet, S. J. Moon, R. H. Baker, P. Gao, M. K. Nazeeruddin, and M. Grätzel, *Nature*, 2013, **499**, 316–319.

[2] J. Cui, F. P. Meng, H. Zhang, K. Cao, H. L. Yuan, Y. B. Cheng, F. Huang, and M. K. Wang, *ACS Appl. Mater. Interfaces*, 2014, **6**, 22862−22870.

[3] W. Chen, Y. Z. Wu, Y. F. Yue, J. Liu, W. J. Zhang, X. D. Yang, H. Chen, E. Bi, I. Ashraful, M. Grätzel, and L.Y. Han, *Science*, 2015, **350**, 944–948.

[4] M. M. Lee, J. Teuscher, T. Miyasaka, T. N. Murakami, H. J. Snaith, Science 338 (2012) 643–647.

[5] M. M. Lee, J. Teuscher, T. Miyasaka, T. N. Murakami, and H. J. Snaith, *Science*, 2012, **338**, 643–647.

[6] C.D. Wagner, L.H. Gale, and R.H. Raymond, *Analytical Chemistry*, 1979, **51**, 466–482.

[7] T. Dutta, P. Gupta, A. Gupta, and J. Narayan, *J. Appl. Phys.*, 2010, **108**, 083715.

[8] Z. H. Bakr, Q. Wali, A. Fakharuddin, L. S. Mende, T. M. Brown, and R. Josea, *Nano Energy*,

2017, **34**, 271–305.

[9] J. Osorio‐Guillén, S. Lany, A. Zunger, Caldas M, and Studart N, *AIP Conference Proceedings. AIP*, 2010, **1199**, 128–129.